CrystEngComm

www.rsc.org/crystengcomm

Volume 15 | Number 20 | 28 May 2013 | Pages 4017–4202

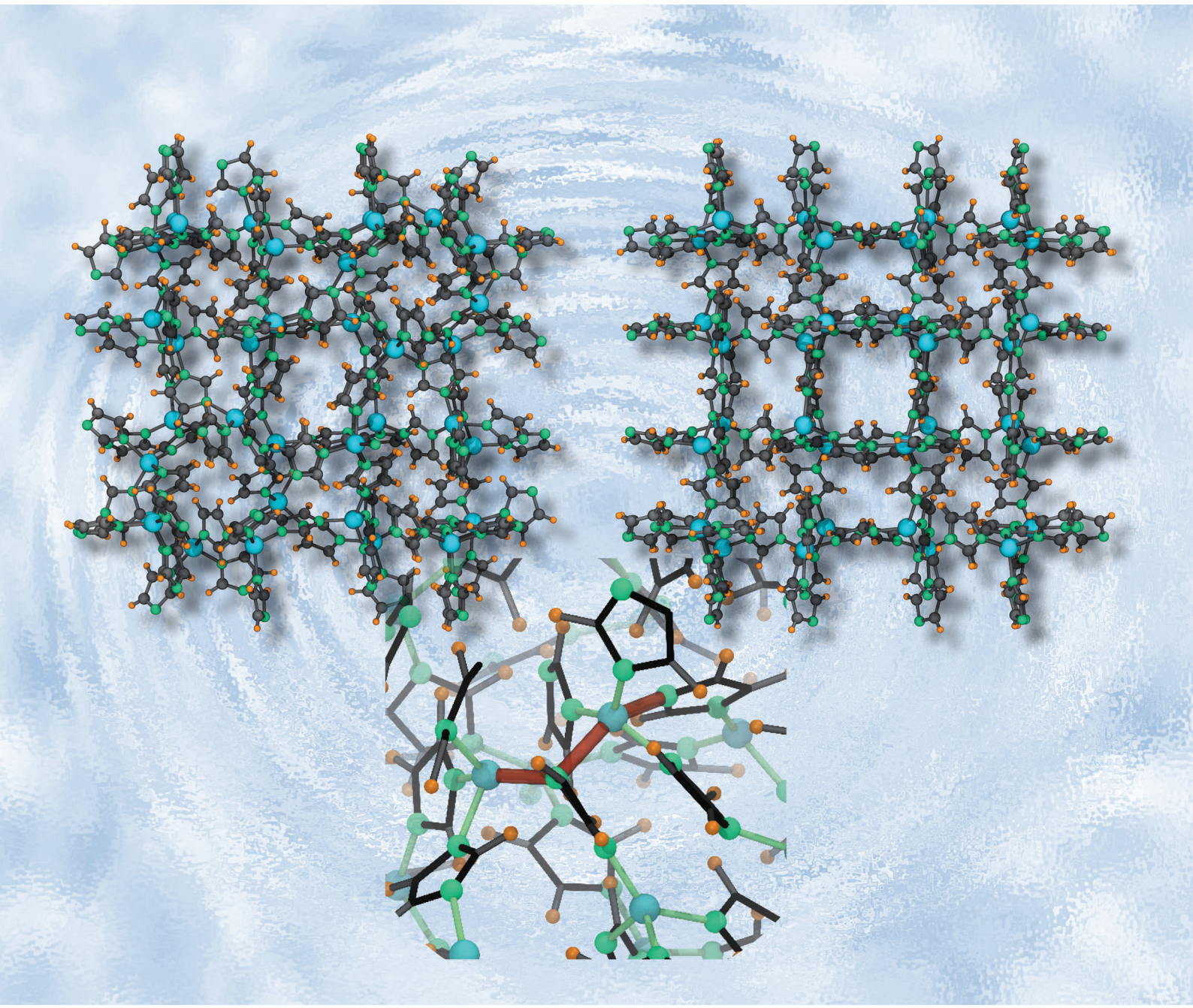

RSC Publishing

COVER ARTICLE

Wiebcke, Leoni *et al*.

Subtle polymorphism of zinc imidazolate frameworks: temperature-dependent ground states in the energy landscape revealed by experiment and theory

CrystEngComm

RSC Publishing

COMMUNICATION

View Article Online
View Journal | View Issue

Subtle polymorphism of zinc imidazolate frameworks: temperature-dependent ground states in the energy landscape revealed by experiment and theory†

Cite this: *CrystEngComm*, 2013, **15**, 4036

Received 2nd July 2012,
Accepted 10th December 2012

DOI: 10.1039/c2ce26045j

www.rsc.org/crystengcomm

Christian A. Schröder,[a] Igor A. Baburin,[b] Leo van Wüllen,[c] Michael Wiebcke*[a] and Stefano Leoni*[b]

We show by variable-temperature X-ray diffraction and differential scanning calorimetry experiments that zinc imidazolates with coi and zni framework topology, respectively represent the thermodynamically stable phase below and above a transition temperature of ≈360 °C at ambient pressure. The relative stability of the two polymorphs and the experimentally observed strong negative thermal expansion of the coi phase at high temperatures close to the phase transition were successfully modelled using density functional theory calculations. A novel metastable zinc imidazolate with neb framework topology was detected by *in situ* X-ray diffraction experiments as a transient crystalline phase during solvothermal crystallisation of the stable coi phase.

Zeolitic imidazolate frameworks (ZIFs) represent a new class of technology relevant microporous materials that are at the focus of current research efforts.[1,2] Important characteristics of ZIFs are comparatively high thermal and chemical stabilities and the ability to crystallise in a large variety of topologically different frameworks which may be tailored for a specific application in gas storage, separation, sensing or catalysis. ZIFs consist of tetrahedral cationic centres (Zn^{II}, Co^{II}, Fe^{II}, Cd^{II}, and also Li^{I}/B^{III}) connected by imidazolate-based bridging ligands. Because of the local tetrahedral geometry of metal connectors and the metal–imidazolate–metal bridging angle of ≈145° ZIFs adopt network topologies common for microporous silica polymorphs and zeolites. Recent studies have revealed that ZIFs may undergo thermally- and/or pressure-induced amorphisation that reinforces the similarity between ZIFs and silica.[3–5] However, important differences between ZIFs and silica systems are still ignored in the literature. For example, it is well known that the thermodynamic 'ground state' of the silica system at ambient conditions corresponds to the α-quartz phase (**qtz** net)[6], whereas the quartz-like topology is hardly accessible in the $Zn(im)_2$ (im = imidazolate) system as was shown in our previous *ab initio* study.[7,8] By considering only unsubstituted imidazolate bridging ligands, nine topologically different $Zn(im)_2$ frameworks have been experimentally realised to date (**zni**, **coi**, **cag**, **mer**, **gis**, **dft**, **crb**, **zec**, **nog**)[1,2,9] and even more are predicted to be synthetically accessible.[7]

However, up to now there was no experimental study which addressed the important question about the thermodynamically most stable phase(s) ('ground state(s)') in the $Zn(im)_2$ system, which might be either of the two most dense phases **zni** or **coi**. Recently, an irreversible single-crystal-to-single-crystal pressure-induced phase transition from the **zni** to the **coi** phase was observed at room temperature by Spencer *et al.*[10] revealing that **coi** is stable at high pressures (≳0.55 GPa). The polymorphs with **zni** and **coi** underlying nets crystallise in the tetragonal space groups $I4_1cd$ and $I4_1$, respectively, and are closely related to each other since both frameworks may be considered as being built up from triple helices connected in different ways (Fig. 1). By now, the **coi** phase was disregarded in theoretical calculations and the **zni** phase was assumed to be the most stable phase.[7,8,11,12] In this Communication, we address the question of the 'ground state' in the $Zn(im)_2$ system from both an experimental and computational point of view.

Variable-temperature X-ray diffraction (XRD) patterns taken from **coi** powder samples at ambient pressure reveal that a phase transition to **zni** takes place at ≈360 °C (Fig. 2a). The **zni** phase decomposes in air at ≈410 °C. On differential scanning calorimetry (DSC) curves measured during heating of **coi** powder an endothermic peak is seen at 349.0 °C (Fig. 2b) in reasonable agreement with the XRD data when considering the different heating rates. The endothermic transition enthalpy proves that the **coi** phase is the thermodynamically stable phase below the transition temperature, *i.e.* the **coi** phase represents the low-temperature and the **zni** phase represents the high-temperature

[a]*Institut für Anorganische Chemie, Leibniz Universität Hannover, Callinstrasse 9, 30167 Hannover, Germany. E-mail: michael.wiebcke@acb.uni-hannover.de; Fax: +49 511 7623006; Tel: +49 511 7623698*

[b]*Institut für Physikalische Chemie und Elektrochemie, Technische Universität Dresden, Mommsenstrasse 13, 01062 Dresden, Germany. E-mail: stefano.leoni@chemie.tu-dresden.de; Fax: +49 351 46335953; Tel: +49 351 46339449*

[c]*Institut für Physik, Universität Augsburg, Universitätsstrasse 1, 86159 Augsburg, Germany*

† Electronic supplementary information (ESI) available: Computational and experimental details, XRD patterns, TG–DTA curves, crystal structure data. CCDC 889150. For ESI and crystallographic data in CIF or other electronic format see DOI: 10.1039/c2ce26045j

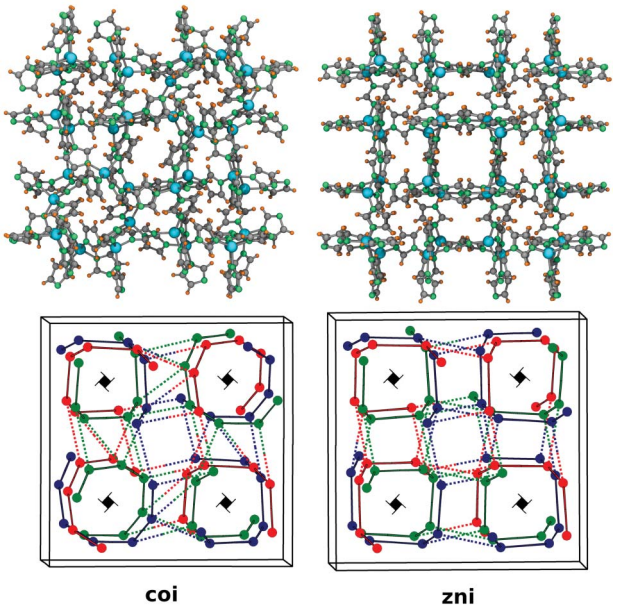

Fig. 1 Top: crystal structures of $Zn(im)_2$ with **coi** (left) and **zni** (right) topologies viewed along the crystallographic *c* axis. Bottom: underlying nets **coi** and **zni** with the bonds responsible for distinguishing them (shown as dotted lines). Triple helices are indicated.

phase at ambient pressure. This is in line with the reported room-temperature densities ($\rho_{\mathbf{coi}} > \rho_{\mathbf{zni}}$).[10] The phase transition is irreversible and the resultant **zni** phase can be recovered at room temperature. The experimental transition enthalpy of the **coi**–**zni** transition determined by DSC amounts to $\Delta H_{exp} = 2.9(1)$ kJ mol^{-1} being in fair agreement with the value obtained by density functional theory (DFT) calculations [$\Delta H_{PBE} = 5.8$ kJ mol^{-1}]. Commonly used generalized gradient approximation (GGA) functional (PBE) allowed for good geometry descriptions of the **coi** and **zni** structures (see ESI†) and yielded an energy difference of $\Delta E_{\mathbf{zni-coi}} = 0.06$ eV/[$Zn(im)_2$] (at 0 K). However, to achieve a quantitative agreement with experimental values, the enthalpy difference was estimated with the recently developed non-local van der Waals DFT functional (see ESI†) being capable of describing dispersion forces, which are important to properly account for inter-ligand interactions.[12] The enthalpy difference in this case amounts to $\Delta H_{vv10} = 1.6$ kJ mol^{-1}, and is in good agreement with the experimental value.

The reflections in the variable-temperature XRD patterns (Fig. 2a) show that the **coi** phase undergoes structural changes with changes in temperature. The variation of the unit cell parameters as a function of temperature is presented in Fig. 3a. Up to ≈280 °C the cell volume slightly increases with temperature. This results from an increase of the tetragonal *a* (and *b*) axis while the *c* axis is constantly decreasing. Strikingly, above ≈280 °C up to the phase transition at ≈360 °C the cell volume strongly shrinks due to contraction of the *c* as well as the *a* axes. At the **coi**–**zni** transition the cell axes change by $\Delta a = +0.490$ Å (2.15%) and $\Delta c = -0.654$ Å (−5.12%) resulting in a small contraction of the cell volume by $\Delta V = -67$ Å^3 (−1.0%), *i.e.* **zni** becomes the most dense phase above ≈360 °C.

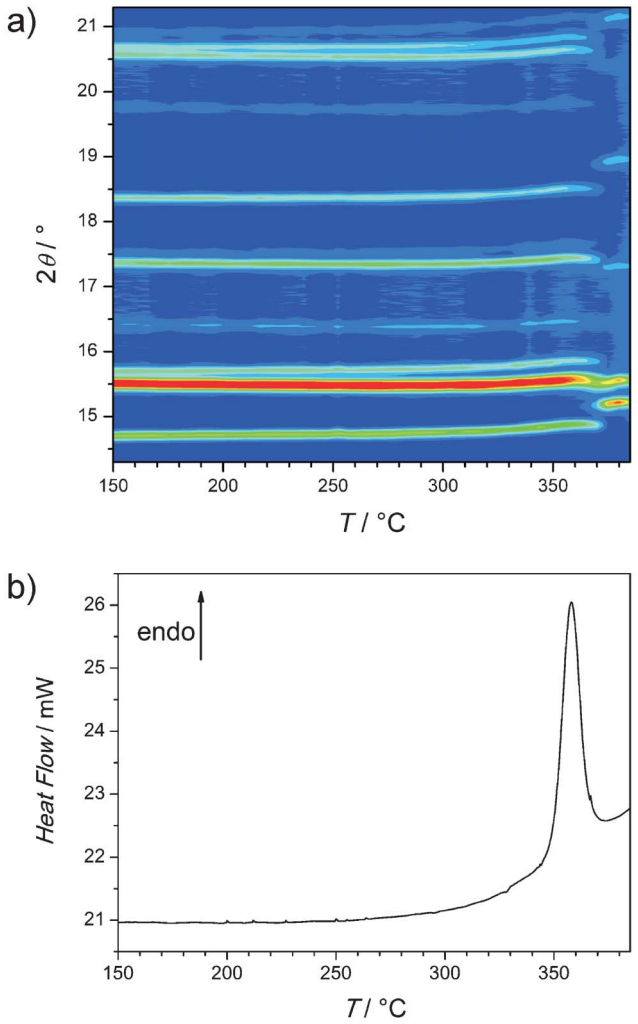

Fig. 2 (a) Variable-temperature XRD patterns collected during heating of a **coi** powder sample. (b) Corresponding DSC curve of a **coi** powder sample.

Note that negative thermal expansion (NTE) is more commonly found/predicted for microporous zeolites and metal–organic frameworks (MOFs).[15–19] For example, the cubic MOF HKUST-1 shows as an isotropic linear coefficient of the thermal expansion of $\alpha_L = dL/(LdT) = -4.1 \times 10^{-6}$ K^{-1}.[16] In contrast, in the temperature range 310–350 °C **coi** has near-linear thermal expansion coefficients parallel to the *a* and *c* axis of $\alpha_a = -112 \times 10^{-6}$ K^{-1} and $\alpha_c = -188 \times 10^{-6}$ K^{-1}, respectively (Fig. 3b). The values are nearly two orders of magnitude more negative than that for HKUST-1 and close to the maximum NTE behaviour reported so far for framework materials.[19]

This interesting thermal behaviour was investigated with constant temperature, constant pressure *ab initio* molecular dynamics (MD) simulations. MD runs were performed at different temperatures in the experimentally relevant range 227–377 °C. Based on a 272 atom primitive cell the cell volume was found to expand as a function of temperature in the lower temperature range in agreement with experiment. The calculations at 347 °C show a tendency towards lengthening (some of) the Zn–N

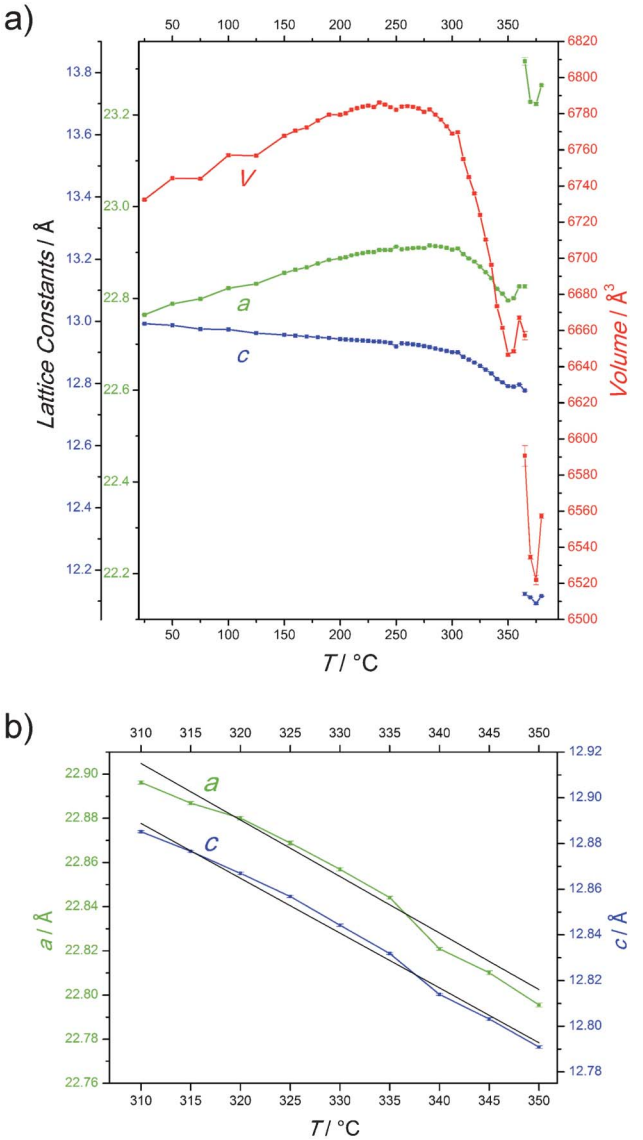

Fig. 3 (a) Evolution of the lattice constants (*a*, *c*) and cell volume (*V*) of the **coi** phase as a function of temperature. (b) Lattice constants (*a*, *c*) *versus* temperature in the range 310–350 °C with linear regression lines (black).

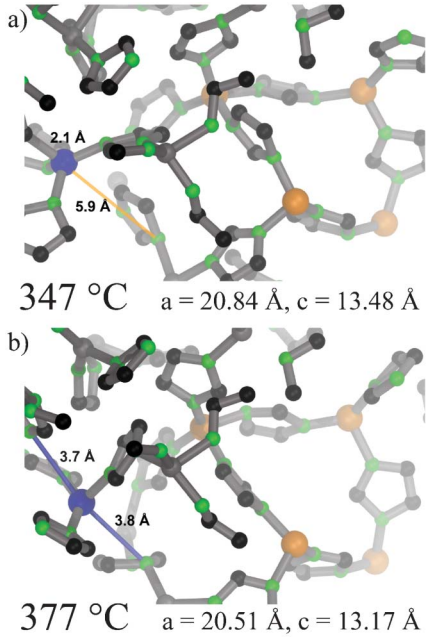

Fig. 4 Two representative geometries of **coi** obtained from isothermic, isobaric MD simulations at two different temperatures (347 °C (a) and 377 °C (b)). Some relevant average Zn–N distances are indicated for a Zn centre (violet colour) that experience bond rearrangement in the course of the **coi**–**zni** transition. Colour code for remaining atoms: orange, Zn; green, N; black, C. H atoms are omitted.

coordination bonds and the formation of trigonal–pyramidal centres (Fig. 4a) and at 377 °C the formation of 'trigonal' coordination environments (Fig. 4b). In the latter geometry one ligand has left and another ligand has not yet entered the coordination sphere. Both the *a* and *c* axes shrink in response to this. This effect is coupled with changes (typically, shortenings) in H···H distances, which are the most relevant non-bonding interactions in the system, as evidenced by monitoring their evolution during MD runs (see ESI†). On forming 'trigonal' centres the axis shortening ratio amounts to $\Delta a/\Delta c = 1.06$ (see ESI†) which is in very good agreement with the corresponding ratio of the experimental data of $\Delta a/\Delta c = (a_{350} - a_{310})/(c_{350} - c_{310}) = 1.1$ (Fig. 3b). Rather than a partial amorphisation process the appearance of 'trigonal' centres is an intermediate stage of the transition into the **zni** phase. In fact, 'trigonal' Zn centres are characteristic of the upper temperature region and are restored to tetrahedral Zn centres on lowering temperature (227 °C) as indicated by our numerical simulations.

The **coi**–**zni** transformation mechanism suggested by our MD simulations involves rearrangement of the same Zn–N contacts as proposed recently by Spencer *et al.*[10] for the pressure-induced **zni**–**coi** transition. Our simulations and experiments now add important mechanistic details about the transition state for the thermally-induced **coi**–**zni** transition. First, the mechanism is broken into simpler steps, *i.e.* the formation of 'trigonal' centres is favoured. Second, ligand substitution in the coordination sphere of Zn is accompanied by volume contraction. Indeed, volume contraction is necessary to shorten inter-ligand distances (particularly, H···H contacts) while covalent bonds of the ligands are not affected by the contraction. As a result, by approaching each other, a ligand can push another one out of the coordination sphere of Zn atoms. A complete transition requires a one ligand switch in the coordination spheres of 4 (out of 16) Zn atoms in the primitive cell (ESI,† Fig. S1c). In Fig. 4 average Zn–N distances are indicated. At lower temperatures (347 °C) one Zn–N bond (2.1 Å) is slightly longer than the remaining three (2.0 Å) and a 'non-bonding' Zn–N contact exists at 5.9 Å. In the activated stage (377 °C) two 'non-bonding' Zn–N contacts fall below 3.8 Å, which allows for ligand reshuffling. The longer 'non-bonding' distances ($\approx$6 Å) at lower temperatures make Zn tetrahedron inversion unlikely.

The mechanistic insight into the phase transition obtained from theory is also of interest with regard to the recently reported thermally-induced amorphisation of various microporous $Zn(im)_2$ phases (**cag**, **dft**, **bct**) at temperatures of 280–300 °C and the

recrystallisation of amorphous $Zn(im)_2$ to **zni** at ≈360 °C.[3,4] Strikingly, the former and latter temperatures exactly correspond to the beginning of volume contraction of the **coi** phase and the point of crossover of stability of the **coi** and **zni** phases, respectively. Thus, the experimentally observed amorphisation of the **cag**, **dft**, and **bct** phases might have become possible due to a high activation barrier for the nucleation of the stable crystalline **coi** phase below ≈360 °C.

Indeed, our experience with synthesising the **coi** phase from solution shows that its nucleation is a rather unfavourable process while the **zni** phase is readily obtained by precipitation from solution – as a metastable phase – under a wide range of conditions[13] in line with Ostwald's rule of stages. Once the **zni** phase has formed it does apparently not transform into the stable **coi** phase when kept under the mother solution, probably due to low differences in solubility as a result of nearly equal total energies (see above). Only very few wet-chemical synthetic protocols for **coi** have been reported.[14,20] We synthesised the **coi** phase according to a recent report[14] under solvothermal conditions from ethanol–pyridine mixture solutions which are rather specific conditions. Thereby, we discovered for the first time that **coi** formation involves the transient crystallisation of a novel phase. According to powder and single-crystal XRD and TG studies this novel metastable phase possesses the composition $[Zn(im)_2 \cdot 0.5py]$ (py = pyridine) and **neb** framework topology (see ESI†). Only a Co analogue had been reported before.[14] The **neb** phase forms at room temperature within a period of about 10 to 120 minutes depending on the composition of the reaction mixture. Upon solvothermal treatment at about 140 °C the intermediate **neb** phase converts with release of pyridine into the stable **coi** phase (see ESI†). This was monitored *in situ* by time-resolved energy-dispersive X-ray diffraction (EDXRD)[21,22] experiments.

As can be seen from the EDXRD spectra and corresponding extent of reaction data (Fig. 5) the conversion takes place rather sharply and involves the dissolution of a significant fraction (≈0.5) of the intermediate **neb** phase before **coi** starts crystallising, suggesting that the conversion is not a solid–solid transformation but rather a solution–mediated recrystallisation process as might be expected from the different framework topologies and chemical compositions. While crystalline intermediates during ZIF formation have been reported previously,[9,23] this is the first direct *in situ* monitoring of a ZIF conversion process in solution. We speculate that nucleation of the **coi** phase takes place heterogeneously on the surfaces of still available **neb** particles. This was indicated by the observation that pure-phase **coi** was only obtained if the **neb**-containing suspension was vigorously stirred (as during the EDXRD experiments). Solvothermal treatment of unstirred solutions yielded under otherwise similar conditions mixtures of **coi** and **zni** (see ESI†). This suggests that stirring leads to close contact between the surfaces of the **neb** particles and the solution and thereby favours the nucleation of the **coi** phase. An alternative explanation might be that due to stirring, the overall level of supersaturation is kept low allowing homogeneous nucleation of the stable (less soluble) **coi** phase while simultaneously excluding nucleation of the metastable (more soluble) **zni** phase because higher levels of local supersaturation are avoided. Either reasoning could explain the difficulties of preparing the stable **coi** phase. It is also difficult to prepare the **coi** phase *via* thermal treatment of the novel **neb** phase in the solid state. TG and variable-temperature XRD studies (see ESI,† Fig. S7 and S8) revealed that during escape of pyridine molecules the **neb** framework structure collapses yielding, besides **coi**, an amorphous material and **zni**.

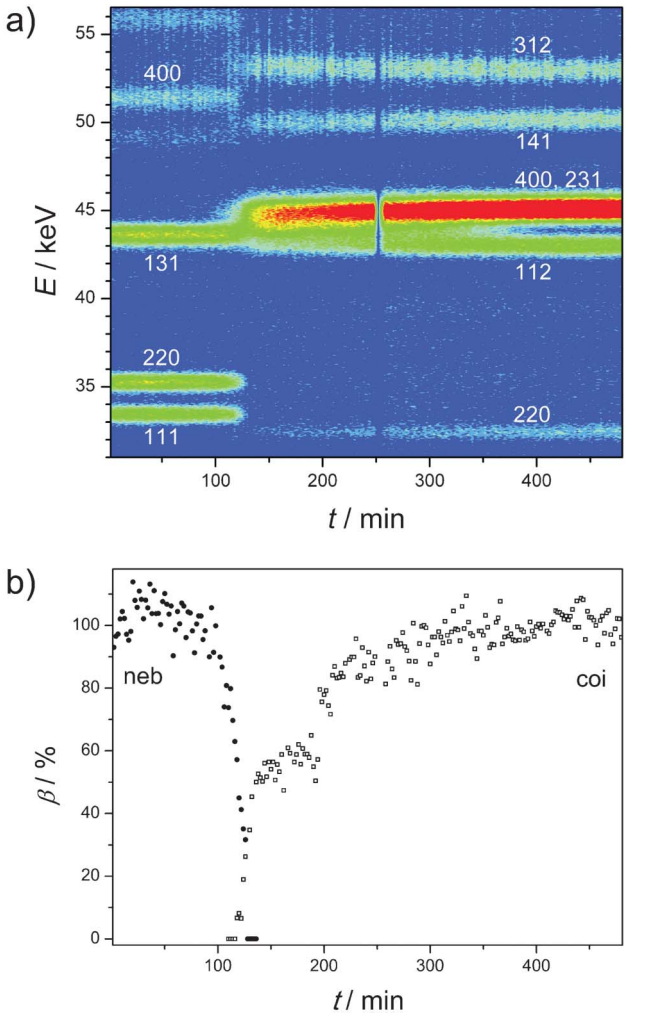

Fig. 5 (a) EDXRD spectra measured during solvothermal treatment at 140 °C of a **neb**-containing synthesis mixture as a function of time. The conversion of **neb** to **coi** takes place after ≈120 min. (The missing data at ≈250 min is due to refilling of the storage ring). Indices *hkl* of Bragg reflections are indicated. (b) Corresponding reaction extents (β) for dissolution of the **neb** and crystallisation of the **coi** phase as a function of time (t). The β values were determined by normalizing the integrated intensities of the 111/220 (**neb**) and 400/231 and 112 (**coi**) reflections to the respective maximum integrated intensities. (The anomaly at about 200 min seen in the extent of crystallisation of **coi** is caused by overlapping of the 400/231 and 112 reflections and resulting problems with profile fitting and accurately extracting the single peak intensities.)

In conclusion, our joint experimental and computational studies have clarified that in the $Zn(im)_2$ system the **coi** and **zni** phases, respectively, represent the thermodynamically stable phase below and above a transition temperature of ≈360 °C at ambient pressure. Therefore, it is reasonable to assume that above

the transition temperature the pressure-induced **zni–coi** phase transition should not take place, *i.e.* the role of the pressure would be mimicked by increased temperature and the accompanying volume reduction. The experimentally observed strong NTE of the **coi** phase at high temperatures close to the phase transition was successfully modelled by DFT calculations and related to the role of inter-ligand interactions which are mainly affected by the volume reduction and finally induce the phase transition by forming 'trigonal' Zn centres, a reactive step towards the transition to the **zni** phase. A novel metastable **neb** phase was detected as a transient phase during solvothermal crystallisation of the stable **coi** phase. The results presented here significantly advance our understanding of the $Zn(im)_2$ and possibly other ZIF systems with regard to phase stabilities, phase transitions and phase formation (synthesis).

Acknowledgements

We thank DESY for provision of beam time at F3 and W. Bensch and his group for providing the heating device used at F3. The work was financially supported by the DFG-SPP 1415 "Crystalline Non-equilibrium Phases" (WI1156/3-1, LE2479/3-1). SL thanks the KCL, London, for hospitality.

References

1 A. Phan, C. J. Doonan, F. J. Uribe-Romo, C. B. Knobler, M. O'Keeffe and O. M. Yaghi, *Acc. Chem. Res.*, 2010, **43**, 58.
2 J.-P. Zhang, Y.-B. Zhang, J.-B. Lin and X.-M. Chen, *Chem. Rev.*, 2012, **112**, 1001.
3 T. D. Bennett, A. L. Goodwin, M. T. Dove, D. A. Keen, M. G. Tucker, E. R. Barney, A. K. Soper, E. G. Bithell, J.-C. Tan and A. K. Cheetham, *Phys. Rev. Lett.*, 2010, **104**, 115503.
4 T. D. Bennett, D. A. Keen, J.-C. Tan, E. R. Barney, A. L. Goodwin and A. K. Cheetham, *Angew. Chem., Int. Ed.*, 2011, **50**, 3067.
5 T. D. Bennett, P. Simoncic, S. A. Moggach, F. Gozzo, P. Macchi, D. A. Keen, J.-C. Tan and A. K. Cheetham, *Chem. Commun.*, 2011, **47**, 7983.
6 M. O'Keeffe, M. A. Peskov, S. J. Ramsden and O. M. Yaghi, *Acc. Chem. Res.*, 2008, **41**, 1782.
7 I. A. Baburin, S. Leoni and G. Seifert, *J. Phys. Chem. B*, 2008, **112**, 9437.
8 I. A. Baburin, B. Assfour, G. Seifert and S. Leoni, *Dalton Trans.*, 2011, **40**, 3796.
9 Y.-Q. Tian, Y.-M. Zhao, Z.-X. Chen, G.-N. Zhang, L.-M. Weng and D.-Y. Zhao, *Chem.–Eur. J.*, 2007, **13**, 4146.
10 E. C. Spencer, R. J. Angel, N. L. Ross, B. E. Hanson and J. A. K. Howard, *J. Am. Chem. Soc.*, 2009, **131**, 4022.
11 D. W. Lewis, A. R. Ruiz-Salvador, A. Gómez, L. M. Rodriguez-Albelo, F.-X. Coudert, B. Slater, A. K. Cheetham and C. Mellot-Draznieks, *CrystEngComm*, 2009, **11**, 2272.
12 R. Galvelis, B. Slater, A. K. Cheetham and C. Mellot-Draznieks, *CrystEngComm*, 2012, **14**, 374.
13 T. Hikov, C. A. Schröder, J. Cravillon, M. Wiebcke and K. Huber, *Phys. Chem. Chem. Phys.*, 2012, **14**, 511.
14 Y.-Q. Tian, C.-X. Cai, X.-M. Ren, C.-Y. Duan, Y. Xu, S. Gao and X.-Z. You, *Chem.–Eur. J.*, 2003, **9**, 5673.
15 P. Lightfoot, D. A. Woodcock, M. J. Maplo, L. A. Villaescusa and P. A. Wright, *J. Mater. Chem.*, 2001, **11**, 212.
16 Y. Wu, A. Kobayashi, G. J. Halder, V. K. Peterson, K. W. Chapman, N. Lock, P. D. Southon and C. J. Kepert, *Angew. Chem., Int. Ed.*, 2008, **47**, 8929.
17 D. Dubbeldam, K. S. Walton, D. E. Ellis and R. Q. Snurr, *Angew. Chem., Int. Ed.*, 2007, **46**, 4496.
18 S. S. Han and W. A. Goddard III, *J. Phys. Chem. C*, 2007, **111**, 15185.
19 A. L. Goodwin, M. Calleja, M. J. Conterio, M. T. Dove, J. S. O. Evans, D. A. Keen, L. Peters and M. G. Tucker, *Science*, 2008, **319**, 794.
20 G. A. V. Martins, P. J. Byrne, P. Allan, S. J. Teat, A. M. Z. Slawin, Y. Li and R. E. Morris, *Dalton Trans.*, 2010, **39**, 1758.
21 F. Millange, M. I. Medina, N. Guillou, G. Férey, K. M. Golden and R. I. Walton, *Angew. Chem., Int. Ed.*, 2010, **49**, 763.
22 N. Pienack and W. Bensch, *Angew. Chem., Int. Ed.*, 2011, **50**, 2014.
23 Y.-Q. Tian, L. Xu, C.-X. Cai, J.-C. Wei, Y.-Z. Li and X.-Z. You, *Eur. J. Inorg. Chem.*, 2004, 1039.

